Inorg. Chem. **2007**, *46*, 3231–3235

New Layered Germanide Halides RE_2GeX_2 (RE = Y, Gd; X = Br, I)

Mar'yana Lukachuk, Reinhard K. Kremer, HansJürgen Mattausch, and Arndt Simon*

Max-Planck-Institut für Festkörperforschung, Heisenbergstrasse 1, D-70569 Stuttgart, Germany

Received December 18, 2006

The title compounds were synthesized from RE, REX_3, and Ge under an Ar atmosphere at 1200–1370 K. Y_2GeI_2 and Gd_2GeI_2 crystallize in space group $R\bar{3}m$ with lattice constants $a = 4.2135(3)$ and 4.2527(1) Å and $c = 31.480(2)$ and 31.657(1) Å, respectively. Gd_2GeBr_2 crystallizes in two modifications, the 1T-type (space group $P\bar{3}m1$; $a = 4.1668(2)$ Å, $c = 9.8173(6)$ Å) and the 3R-type (space group $R\bar{3}m$; $a = 4.1442(9)$ Å, $c = 29.487(7)$ Å). The structural motifs of RE_2GeX_2 compounds are Ge-centered slightly distorted RE_6 octahedra connected via their common edges and extending in the *a* and *b* directions. The resulting close-packed double layers are separated by halogen atoms. The electrical resistivity measurements revealed semiconductor behavior for Y_2GeI_2 and Gd_2GeI_2 and a metal–semiconductor transition for 1T-Gd_2GeBr_2. Magnetic susceptibility and heat capacity measurements show long-range magnetic ordering for Gd_2GeI_2 and 1T-Gd_2GeBr_2 at ∼15 and ∼13 K, respectively.

Introduction

A number of metal-rich rare-earth halides[1−4] crystallize with layered structures resulting from two-dimensional condensation of RE_6 octahedra. These structures relate to those of the binary compounds ZrCl[5,6] and ZrBr.[7] Close-packed bilayers of metal atoms are sandwiched by layers of halogen atoms, forming slabs which are bonded via van der Waals interactions. The metal atom framework leaves voids for different interstitials Z.[1−4,8−15] The resulting RE_2ZX_2 compounds (X = halogen atom) crystallize in trigonal (1T) or rhombohedral (3R) types which differ in the stacking sequence of the slabs. For the 1T type, the translation period corresponds to one slab in the unit cell, whereas the unit cell contains three such slabs for the 3R type. Many RE_2ZX_2 compounds,[8,10−12] depending on the synthesis temperature, were found to crystallize in both 1T and 3R types. Here, the synthesis, structure, and physical properties of three new rare-earth metal germanide halides closely related to La_2GeI_2[11] are reported.

Experimental Section

Preparation. RE metal pieces (RE = Y, Gd) (Alfa Aesar, 99.99%), REX_3 (X = Br, I), and Ge (99.99%) were used as starting materials. Y and Gd were hydrogenated, crushed, and then dehydrogenated under dynamical vacuum ($\leq 10^{-5}$ mbar) at 1070 K (Mo boat, 24 h). The rare-earth trihalides, REX_3, were prepared from the reaction of the oxides (99.9%) with HX and NH_4X and purified twice by sublimation under high vacuum in Ta containers. All handling of the educts and products was carried out under purified Ar either in a glovebox or by using standard Schlenk technique.

Reactions were performed with appropriate mixtures of the starting materials in Ta tubes sealed under an Ar atmosphere, which were subsequently jacketed in silica glass ampules under ca. 10^{-2} mbar vacuum. The synthesis conditions are compiled in Table 1. The 3R type of Gd_2GeBr_2 could only be obtained with a yield of ca. 10%, which could be the result of a narrow temperature range of existence.

Very thin platelike crystals with gold or bronze color were observed for all products. EDX analyses of the reaction products,

* To whom correspondence should be addressed. E-mail: A.Simon@fkf.mpg.de.

(1) Simon, A.; Mattausch, Hj.; Miller, G. J.; Bauhofer, W.; Kremer, R. K. In *Handbook on the Physics and Chemistry of Rare Earths*; Gschneidner, K. A., Jr., Eyring, L., Eds.; North Holland: Amsterdam, 1991; Vol 15, p 191.
(2) Corbett, J. D. *J. Chem. Soc., Dalton Trans*. **1996**, *5*, 575.
(3) Meyer, G. *Chem. Rev*. **1988**, *88*, 93.
(4) Simon, A.; Mattausch, Hj.; Ryazanov, M.; Kremer, R. K. *Z. Anorg. Allg. Chem.* **2006**, *632*, 919.
(5) Izmailovich, A. S.; Trojanov, S. I.; Tsirelnikov, V. I. *Russ. J. Inorg. Chem.* **1974**, *19*, 1597.
(6) Adolphson, D. G.; Corbett, J. D. *Inorg. Chem.* **1976**, *15*, 1820.
(7) Daake, R. L.; Corbett, J. D. *Inorg. Chem.* **1977**, *16*, 2029.
(8) Hwu, S.-J.; Ziebarth, R. P.; von Winbush, S.; Ford, J. E.; Corbett, J. D. *Inorg. Chem.* **1986**, *25*, 283.
(9) Schwanitz-Schüller, U.; Simon, A. *Z. Naturforsch.* **1985**, *40b*, 710.
(10) Schleid, Th.; Meyer, G. *Z. Anorg. Allg. Chem.* **1987**, *552*, 90.
(11) Mattausch, Hj.; Zheng, C.; Ryazanov, M.; Simon, A. *Z. Anorg. Allg. Chem.* **2005**, *631*, 302.
(12) Mattausch, Hj.; Kremer, R. K.; Simon, A. *Z. Anorg. Allg. Chem.* **1995**, *621*, 1001.
(13) Cockcroft, J. K.; Kremer, R. K.; Mattausch, Hj.; Raju, N. P.; Simon, A. *J. Alloys Compd.* **1992**, *183*, 241.
(14) Mattausch, Hj.; Eger, R.; Simon, A. *Z. Anorg. Allg. Chem.* **1991**, *579*, 145.
(15) Schleid, Th.; Meyer, G. *Z. Kristallogr*. **1994**, *209*, 371.

10.1021/ic062425d CCC: $37.00
Published on Web 03/21/2007

Table 1. Experimental Conditions for the Syntheses of the RE_2GeX_2 Compounds

compound	educts	reaction temp (K)	time (days)	estimated yield (%)
Y_2GeI_2	4Y, $2YI_3$, 3Ge	1320	8	>90
Gd_2GeI_2	4Gd, $2GdI_3$, 3Ge	1370	8	90
Gd_2GeBr_2 (1T)	5Gd, $3GdBr_3$, 3Ge	1200	42	70
Gd_2GeBr_2 (3R)	2Gd, $GdBr_3$, Ge	1220	12	~10

using a TESCAN scanning electron microscope with an Oxford EDX detector, confirmed the 2:1:2 atomic ratio of the component elements. All compounds react readily with air and water, resulting in strongly smelling oxidized or hydrolyzed products.

Structure Refinement. X-ray powder diffraction patterns were recorded on a STADI P powder diffractometer (Stoe, Darmstadt), using Ge-monochromatized Mo $K\alpha_1$ radiation ($\lambda = 0.7093$ Å) with carefully ground samples enclosed in sealed glass capillaries. From the powder diffraction patterns, Y_2GeI_2 and Gd_2GeI_2 and the high-temperature form of Gd_2GeBr_2 were found to be isostructural with the 3R-type of Lu_2CCl_2,[10] whereas the low-temperature form of Gd_2GeBr_2 is isostructural with the 1T-type of Gd_2CBr_2.[9] Since the crystals of RE_2GeX_2 are extremely soft and stacked as thin layers, well-shaped specimens suitable for a single-crystal X-ray structure analysis were difficult to prepare. We therefore performed a Rietveld profile refinement using the *FullProf* package.[16] In the refinement, the background was set manually and the reflection profiles were modeled using the pseudo-Voigt function. Although the samples were very well ground and mixed with glass powder to avoid texturing effects, enhanced intensities of the 00*l* and *hhl* reflections were found. A similar result is well-known from early investigations on ZrCl[7] as well as on "t-GdCl" and "t-TbCl"[17] (which were later found out to be hydride chlorides). The effect is only observed with the ZrCl-type layer stacking and not with that of ZrBr. It is obviously due to mechanical introduction of layer disorder.

The plots of the final Rietveld refinements are shown in Figure 1, and the refinement parameters for Y_2GeI_2, Gd_2GeI_2, and 1T-Gd_2GeBr_2 are summarized in Table 2. Because of the small yield of 3R-Gd_2GeBr_2, only the lattice parameters ($a = 4.1442(9)$ Å and $c = 29.487(7)$ Å) could be calculated from a least-squares fit of the powder diffraction data of the selected phase.

The crystallographic information, including the fractional coordinates and selected bond lengths of Y_2GeI_2, Gd_2GeI_2, and 1T-Gd_2GeBr_2, is listed in Tables 2−4.

Physical Properties. For the measurements of the electrical conductivity, the polycrystalline samples were pressed into pellets of 5 mm diameter and ca. 2 mm in thickness. The conventional four-contact van der Pauw method[18] was used. The magnetic susceptibilities of Gd_2GeI_2 and Gd_2GeBr_2 were measured with a MPMS SQUID magnetometer (Quantum Design) using sample quantities of ca. 20 mg. Heat capacities were measured in a PPMS system (Quantum Design) on pressed pellets of ~20 mg. All measurements were carried out on pure RE_2GeX_2 phases selected under an optical microscope and characterized by X-ray powder diffraction.

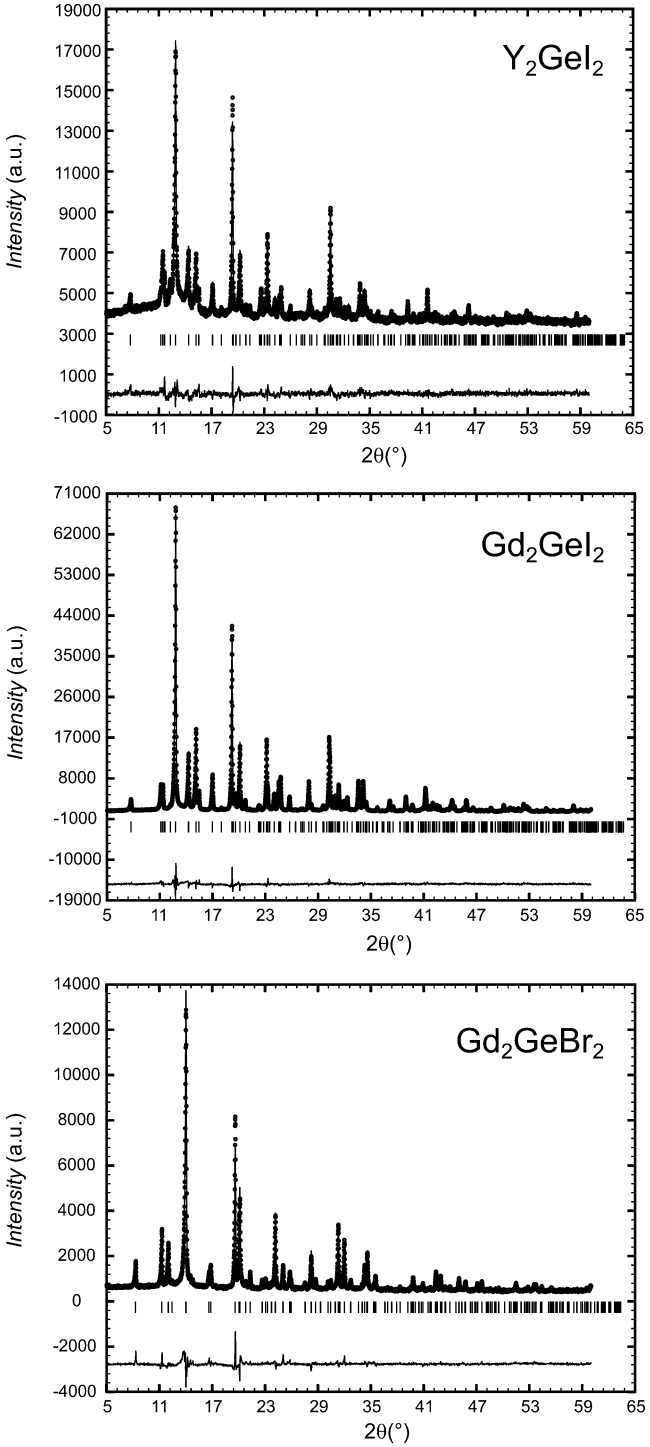

Figure 1. Rietveld refinement plots for Y_2GeI_2, Gd_2GeI_2, and 1T-Gd_2GeBr_2; observed intensities indicated with open circles, calculated patterns with solid lines. The vertical bars indicate the Bragg positions; the difference between observed and calculated patterns is drawn below.

Results and Discussion

The 1T-Gd_2GeBr_2 crystallizes in space group $P\bar{3}m1$ (Figure 2, left). The Br−Gd−Ge−Gd−Br slabs are arranged in a close-packing sequence *aBγAb* along [001]. Y_2GeI_2, Gd_2GeI_2, and 3R-Gd_2GeBr_2 crystallize in the rhombohedral space group $R\bar{3}m$ (Figure 2, right). Their structure consists of the same types of slabs as those in Gd_2GeBr_2, but every next layer is shifted by $^2/_3\ ^1/_3\ ^1/_3$ relative to the previous one. This results in a tripling of the *c* lattice parameter and rhombohedral symmetry. The close-packing sequence is *aBγAb cAβCa bCαBc*.

(16) Rodriguez-Carvajal, J. *FullProf.2k*, version 2.70; CEA-CNRS: Gif-sur-Yvette, France, 2004.
(17) Mattausch, Hj.; Simon, A.; Holzer, N.; Eger, R. *Z. Anorg. Allg. Chem.* **1980**, *466*, 7.
(18) van der Pauw, L. *Philips Res. Rep.* **1958**, *13*, 1.

Table 2. Crystal Structure Data and Rietveld Refinement Parameters for Y_2I_2Ge, Gd_2I_2Ge, and 1T-Gd_2Br_2Ge[a]

empirical formula	Y_2GeI_2	Gd_2GeI_2	1T-Gd_2GeBr_2
fw	504.23	640.91	546.91
temp (K)	293(2)	293(2)	293(2)
wavelength (Å)	0.7093	0.7093	0.7093
cryst syst	rhombohedral		trigonal
space group	$R\bar{3}m$	$R\bar{3}m$	$P\bar{3}m1$
unit cell dimens			
a (Å)	4.2135(3)	4.2527(1)	4.1668(2)
c (Å)	31.480(2)	31.657(1)	9.8173(6)
volume(Å^3), *Z*	484.00(5), 3	495.83(3), 3	147.61(1), 1
density (calcd) (g/cm^3)	5.19	6.44	6.15
no. of collected points, *N*	5800	5800	5800
no. of reflns	265	267	238
no of refined params, *P*	17	17	17
S	1.55	3.10	2.02
final *R* indices			
R_p	0.0179	0.0545	0.0551
R_{wp}	0.0242	0.0706	0.0734
R_{exp}	0.0155	0.0227	0.0363
R_B	0.1064	0.0607	0.0726

[a] $R_p = \sum|y_o - y_c|/\sum|y_o|$, $R_{wp} = [\sum w|y_o - y_c|^2/\sum w|y_o|^2]^{1/2}$, $R_{exp} = [(N - P)/\sum w y_o^2]^{1/2}$, $R_B = \sum|I_o - I_c|/\sum|I_o|$, $S = R_{wp}/R_{exp}$.

Table 3. Atomic Coordinates and Isotropic Displacement Parameters (Å^2) for Y_2GeI_2, Gd_2GeI_2, and 1T-Gd_2GeBr_2

atom	Wyckoff position	*x*	*y*	*z*	*B*
		Y_2GeI_2 ($R\bar{3}m$)			
Y	6*c*	1/3	2/3	0.0499(1)	1.56(7)
I	6*c*	2/3	1/3	0.11287(6)	1.85(5)
Ge	3*a*	0	0	0	1.5(1)
		Gd_2GeI_2 ($R\bar{3}m$)			
Gd	6*c*	1/3	2/3	0.04993(3)	1.52(2)
I	6*c*	2/3	1/3	0.11330(3)	1.89(3)
Ge	3*a*	0	0	0	1.55(5)
		1T-Gd_2GeBr_2 ($P\bar{3}m1$)			
Gd	2*d*	1/3	2/3	0.1657(3)	1.79(5)
Br	2*d*	1/3	2/3	0.6579(4)	1.21(8)
Ge	1*a*	0	0	0	1.2(1)

Table 4. Interatomic Distances (Å) for Y_2GeI_2, Gd_2GeI_2, and 1T-Gd_2GeBr_2

	Y_2GeI_2	Gd_2GeI_2	1T-Gd_2GeBr_2
RE−RE	3.972(4), 4.2135(3)	4.003(1), 4.2527(1)	4.046(3), 4.1668(2)
RE−X	3.139(2)	3.1706(8)	2.964(3)
RE−Ge	2.895(2)	2.9201(5)	2.904(2)
X−X	4.170(2), 4.2135(3)	4.177(1), 4.2527(1)	3.924(4), 4.1668(2)
X−Ge	4.306(2)	4.3466(8)	4.131(3)
Ge−Ge	4.2135(3)	4.2527(1)	4.1668(2)

Since Y_2GeI_2 and Gd_2GeI_2 are isostructural and have the same stacking sequence with respect to the layers as that observed for Gd_2GeBr_2, we describe the interatomic distances only for 1T-Gd_2GeBr_2. The closest Gd−Gd contact is found between the layers (4.05 Å), and it is much longer than the average Gd−Gd distance of 3.60 Å in *hcp* Gd.[19] The metal−metal distance within these layers is somewhat larger (4.17 Å, *a* lattice parameter). In the isotypic Gd_2CBr_2 compound,[9] the Gd−Gd distances (3.43 and 3.82 Å) are much shorter due to the smaller atomic radius of the C atom compared with that of Ge. Despite these differences, the *c* lattice parameters in Gd_2CBr_2 and Gd_2GeBr_2 are almost equal and amount to 9.82 Å.

(19) Donohue, J. *The Structures of the Elements*; Wiley: New York, 1974.

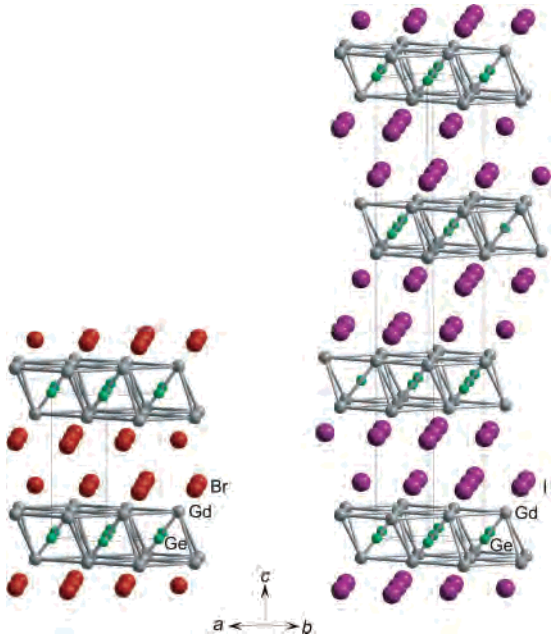

Figure 2. Projections of the 1T-Gd_2GeBr_2 (left) and Gd_2GeI_2 (right) structures.

The shortest distance between the neighboring Ge atoms is 4.17 Å, which is too large for forming Ge−Ge bonds. The Gd−Ge distance of 2.90 Å is only slightly longer than the sum of the covalent radii of Gd and Ge (2.83 Å).[20] As Ge atoms are not bonded to each other, the charge distribution for the RE_2GeX_2 compounds can be approximated in an ionic formulation as $(RE^{3+})_2Ge^{4-}(X^-)_2$ with no valence electrons in the RE framework.

Electrical and Magnetic Properties. Figure 3 shows the results of resistivity measurements for Y_2GeI_2, Gd_2GeI_2, and 1T-Gd_2GeBr_2. The temperature dependence of Y_2GeI_2 and Gd_2GeI_2 indicates semiconducting behavior in the entire temperature range. The room-temperature resistivity of Y_2GeI_2 amounts to about 4 Ω cm and increases by 8 orders of magnitude on cooling to low temperatures. The room-temperature resistivity of Gd_2GeI_2 is 1 order of magnitude smaller (0.1 Ω cm) and increases by 4 orders of magnitude upon lowering of the temperature. 1T-Gd_2GeBr_2 exhibits a semiconducting behavior only at temperatures below ∼150 K with an increase of the resistivity by 2 orders of magnitude. A linear increase of the resistivity above 150 K (see insets of Figure 3) indicates a transition to metallic characteristics. 1T-Gd_2GeBr_2 has the smallest room-temperature resistivity among the title compounds, which amounts to ∼35 mΩ cm. The ρ (logarithmic scale) vs $1/T$ dependences for the title compounds (Figure 3) between approximately 25 and 100 K are almost linear, indicating a thermally activated conduction. The analyses with an Arrhenius law, $\rho(T) \propto \exp(-E_A/k_BT)$, yield activation energies, E_A, of 43, 10, and 3.3 meV for Y_2GeI_2, Gd_2GeI_2, and 1T-Gd_2GeBr_2, respectively.

The magnetic susceptibilities of Gd_2GeI_2 and 1T-Gd_2GeBr_2 (Figure 4) follow a Curie−Weiss law. The experimental effective magnetic moments obtained from the high-temperature slopes of the $1/\chi$ vs T plots amount to 7.98 and

(20) Emsley, J. *The Elements*; Oxford University Press: Oxford, 1989.

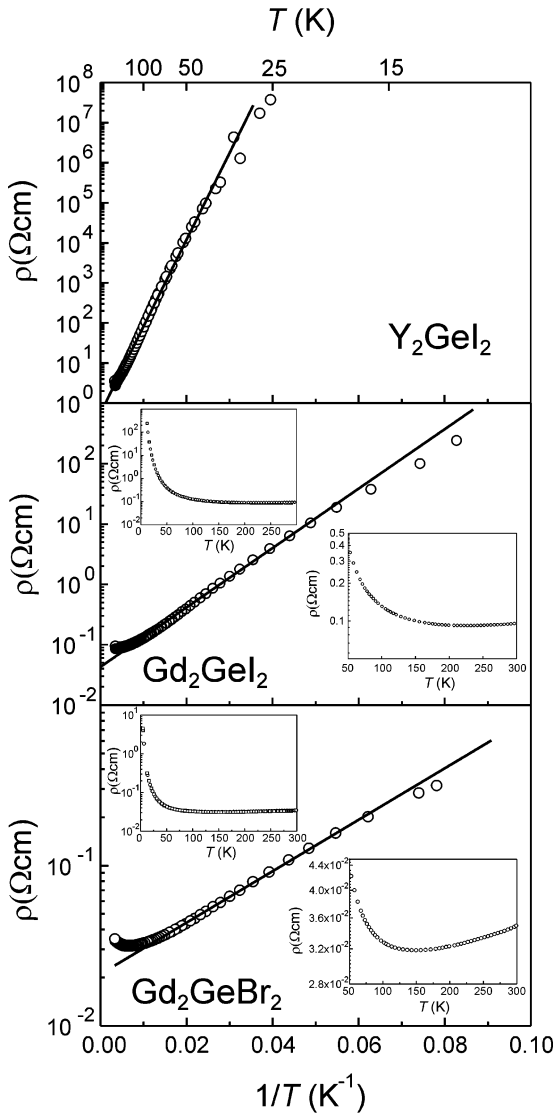

Figure 3. Temperature dependence of the resistivities for Y_2GeI_2, Gd_2GeI_2, and 1T-Gd_2GeBr_2 (from top to bottom).

7.72 μ_B for Gd_2GeI_2 and 1T-Gd_2GeBr_2, respectively. These values are in good agreement with the expected effective moment of 7.94 μ_B for Gd^{3+} with a $^8S_{7/2}$ ground state. The paramagnetic Curie temperatures are negative for both compounds, indicating predominant antiferromagnetic exchange interaction, and they amount to −14 and −11 K for Gd_2GeI_2 and 1T-Gd_2GeBr_2, respectively. Indeed, an antiferromagnetic ordering is indicated by a shallow maximum in the susceptibility with a Néel temperature $T_N \approx 15$ K when sufficiently small external fields of 0.01 or 0.1 T are applied. The maximum is suppressed, and steep ferromagnetic-like increases of the susceptibilities with saturation effects occur as the magnetic field is increased.

The heat capacity data for Gd_2GeI_2 and 1T-Gd_2GeBr_2 (Figure 5a) show λ-type anomalies at ∼15 K for Gd_2GeI_2 and ∼13 K for 1T-Gd_2GeBr_2, indicating long-range magnetic ordering. Comparison with the heat capacity of the nonmagnetic compound Y_2GeI_2 reveals that the magnetic contributions to the specific heat for Gd_2GeI_2 and 1T-Gd_2GeBr_2 are dominant below ∼10 K and extend up to ∼70 K. However, the majority of the magnetic contributions is concentrated

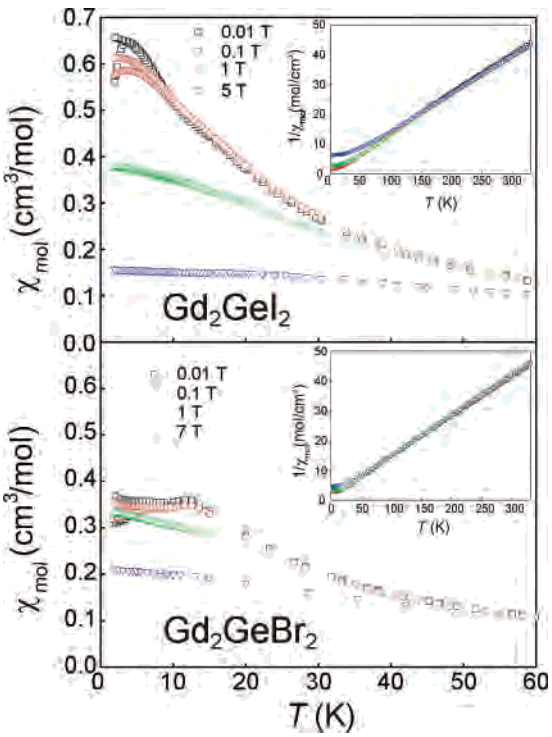

Figure 4. Magnetic susceptibilities of Gd_2GeI_2 and 1T-Gd_2GeBr_2. The insets show the inverse magnetic susceptibilities.

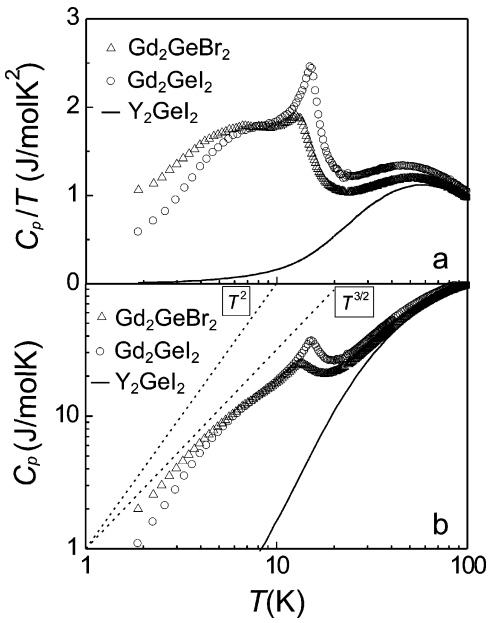

Figure 5. Heat capacities of Gd_2GeI_2, 1T-Gd_2GeBr_2, and Y_2GeI_2 presented as C_p/T vs T (a) or C_p vs T (b). The dashed lines in part b indicate a power-law behavior $C_p \propto T^2$ or $C_p \propto T^{3/2}$.

below the ordering temperatures. These contributions are stronger for 1T-Gd_2GeBr_2 than for Gd_2GeI_2. Accordingly, the magnitude of the λ anomaly of 1T-Gd_2GeBr_2 is somewhat reduced, and a large fraction of the magnetic entropy is shifted below the ordering temperature. Similar low-temperature ($T < T_N$) features in the magnetic heat capacity were observed, e.g., in $GdIH_x$ ($0.66 \leq x \leq 0.86$).[21] We attribute

(21) Ryazanov, M.; Kremer, R. K.; Simon, A.; Mattausch, Hj. *Phys. Rev.* **2006**, *B73*, 035114.

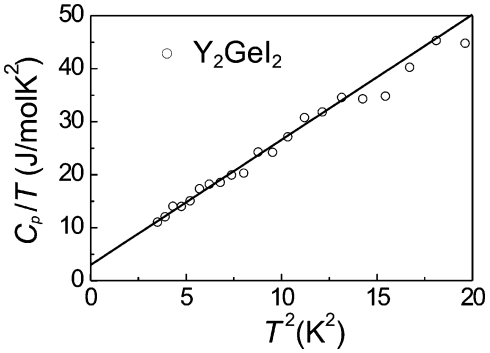

Figure 6. Sommerfeld plot Y_2GeI_2 below 4 K.

these features to complex-canted antiferromagnetic order as a result of the competing interactions in the triangular RE layers.

Below the ordering temperature, the magnetic heat capacity of Gd_2GeI_2 follows a T^2 behavior (Figure 5b), which can be attributed to the magnon heat capacity of a two-dimensional antiferromagnetic system. In contrast, the magnetic contribution to the heat capacity of 1T-Gd_2GeBr_2 decreases with a power-law behavior $C_{mag} \propto T^{3/2}$ common for spin waves in a three-dimensional ferromagnet.

The heat capacity data of Y_2GeI_2 between 2 and 4 K are presented as a C_p/T vs T^2 plot in Figure 6. In this temperature range, the lattice and electronic contributions can be described by the sum of a Debye βT^3 term and a linear Sommerfeld γT term according to

$$C_p = \gamma T + \beta T^3 \qquad (1)$$

with the Sommerfeld coefficient $\gamma = 3.0(6) \times 10^{-3}$ J/mol K^2 and $\beta = 2.36(8) \times 10^{-3}$ J/mol K^4. The coefficient β corresponds to a Debye temperature of $\Theta_D(0) = 160$ K. This value lies well in the range of similar compounds, e.g., $YIH_{0.8}$ $\Theta_D(0) = 220$ K.[22] A linear contribution to the heat capacity is unexpected in view of the semiconducting behavior of Y_2GeI_2. It may be due to disorder or some doping-induced charge carriers. For example, in Si single crystals, similar values were observed, which were ascribed to a doping level of 10^{20} atoms/cm^3.[23,24]

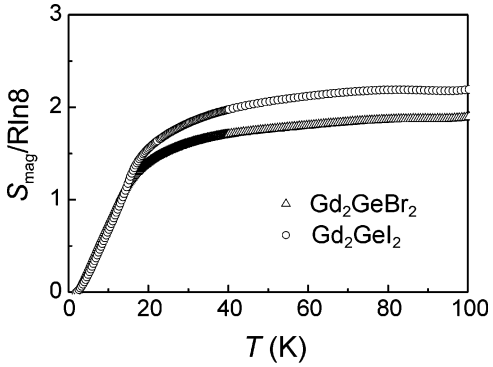

Figure 7. Temperature dependence of the magnetic entropies, S_{mag}, of Gd_2GeI_2 and 1T-Gd_2GeBr_2.

The spin entropies $S_{mag}(T)$ of Gd_2GeI_2 and 1T-Gd_2GeBr_2, calculated according to

$$S(T) = \int_0^T \frac{C_{mag}(T')}{T'} \, dT' \qquad (2)$$

are plotted in Figure 7. To obtain the magnetic contributions C_{mag} for the Gd compounds, C_p of Y_2GeI_2 was subtracted as a reference for the phonon contributions. The different atomic masses of Gd and Y and the different stacking sequences in the crystal structures of Gd_2GeI_2 and 1T-Gd_2GeBr_2 will certainly cause some changes in the phonon spectrum and a slight difference of the lattice heat capacities. However, as can be seen in Figure 5b, the heat capacity of Y_2GeI_2 at high temperatures approaches rather well the C_p values of Gd_2GeI_2 and 1T-Gd_2GeBr_2 despite the Y−Gd mass difference. To compensate for the mass differences of Y and Gd, an empirical factor of 1.09 was applied to adjust the heat capacities of Y_2GeI_2 and Gd_2GeX_2 at high temperature, where no magnetic contributions are present. The entropy increases steeply and levels off at temperatures ∼15 K, where the magnetic orderings occur. About 75% of the magnetic entropy is removed below T_N, indicating that short-range magnetic ordering effects with sizable contributions to the heat capacities above T_N are not observed. The saturation value of the entropy is very close to $2R$ ln 8, as expected for a system with two Gd^{3+} ($S = {}^7/_2$) atoms per formula unit.

Acknowledgment. We thank E. Brücher and G. Siegle for the magnetization and resistivity measurements.

Supporting Information Available: Three CIF files. This material is available free of charge via the Internet at http://pubs.acs.org.

IC062425D

(22) Ryazanov, M.; Kremer, R. K.; Simon, A.; Mattausch, Hj., unpublished results.
(23) Gibin, A.; Devyatykh, G. G.; Gusev, A. V.; Kremer, R. K.; Cardona, M.; Pohl, H.-J. *Solid State Commun.* **2005**, *133*, 569.
(24) Keesom, P. H.; Seidel, M. *Phys. Rev.* **1959**, *113*, 33.